

## GRAVITATIONAL TIDES IN THE OUTER PLANETS. II. INTERIOR CALCULATIONS AND ESTIMATION OF THE TIDAL DISSIPATION FACTOR

PETROS J. IOANNOU AND RICHARD S. LINDZEN

Center for Meteorology and Physical Oceanography, Massachusetts Institute of Technology, Cambridge, MA 02139

Received 1992 June 25; accepted 1992 September 22

## ABSTRACT

The theory of excitation of tidal oscillations in a fluid planetary body is formulated, and separable equations are derived that extend the results of the classical theory of tides to the nonhydrostatic interiors of planets. The theory is applied to the example of the gravitational tidal response of Jupiter to forcing by Io. The tidal response is found to crucially depend on the static stability in the interior of the planet, the response of the planet being as much as two to three orders of magnitude greater than the response with a neutral interior. The tidal dissipation factor  $Q$  is calculated for Jupiter and found to agree with the values required by the astronomical arguments only if the interior has finite (though small static stability). We are led to the conclusion that the interior of Jupiter must have regions which are stably stratified.

*Subject headings:* planets and satellites: individual (Jupiter)

## 1. INTRODUCTION

Jupiter has a rotational period of 9.92 hr and a radius approximately 10 times greater than Earth's and 10 times smaller than the Sun's. The main constituents of the planet, hydrogen (90% by mass) and helium (10%), do not solidify, and because of the low density the mass of the planet is only 318 times greater than Earth's. The planet is primarily made up of a highly compressed but relatively cold liquid, with an interior core at probably 0.1 of the planetary radius. The visible atmospheric envelope is approximately at a pressure of 1 bar and a temperature of 150 K, while the pressure at the core is approximately 40 Mbar at a temperature of nearly 20,000 K (Stevenson 1978). Observations on the thermal emission revealed the existence of an interior heat source which accounts for around 35% of the  $14 \text{ W m}^{-2}$  emitted to space.

While much progress has been made in our understanding of the general structure of the planet (cf. Stevenson 1978), most of the meteorologically relevant information is limited to the region above the visible clouds of the planet. The data for the meteorology of the planet is still scant, making the theories for the observed cloud level circulations speculative (Ingersoll 1990).

It was suggested recently (Ioannou & Lindzen 1993, hereafter IL) that the excitation of the outer planets by the gravitational tidal potential of their satellites may prove to be a useful probe of the planetary structure. The planets are subjected to a forcing of known magnitude and frequency, and observation of the response provides information about the mean thermodynamic structure. The gravitational forcing is distributed throughout the planet, and the response in the atmosphere, concentrated in the higher Hough modes, will crucially depend on the excitation in the interior. It is the purpose of this paper to formulate the theory of tidal excitation of Jupiter by Io, the satellite that dominates the time-varying Jovian tidal potential (see IL).

One of the most important unknowns for the meteorology of the planet is the distribution of static stability below the visible clouds. It is widely assumed that the internal heat source of the planet convectively adjusts the deep atmosphere to a neutrally buoyant state. Under this assumption the interior responds

weakly to imposed gravitational tidal driving (Houben & Gierasch 1977; Houben 1978). We relax the assumption of exact neutrality in the interior and find that the tidal response is markedly enhanced even for small values of the stratification.

Associated with the excitation of tides is the long-standing problem of determining the tidal dissipation which is responsible for the evolution of the orbits of the satellites (Darwin 1910). Observations of the rate of tidal dissipation can provide a clue to the interior stability structure of the planet. Briefly, when the rotation period of the planet is smaller than the orbital period of the satellite, the tidal dissipation is associated with a torque that decreases the rotation period of the planet, leading to an increase in the angular momentum of the satellite by a factor denoted by  $A$ , where  $A > 1$ . If the satellite is in a prograde orbit around the planet, its resulting angular momentum will be

$$\omega_s D^2 = A \omega_{s,0} D_0^2, \quad (1.1)$$

where  $2\pi/\omega_s$  is the new orbital period of the satellite and  $D$  its new distance from the planet, and the subscript "0" denotes the corresponding initial values. Kepler's third law

$$\omega_s^2 D^3 = \omega_{s,0}^2 D_0^3 \quad (1.2)$$

and equation (1.1) lead to

$$D = A^2 D_0, \quad (1.3)$$

$$\omega_s = A^{-3} \omega_{s,0}. \quad (1.4)$$

Consequently the orbit of a prograde satellite will expand, and the orbital period will increase. The opposite is true for retrograde satellites. The rate of expansion depends on the angular momentum transfer  $A$ , which in turn is an increasing function of the tidal dissipation. Because of this effect the present location of the satellites of a planet provides a bound on the average tidal dissipation in the planet.

Tidal friction is measured by the quality factor  $Q$  defined by Goldreich & Soter (1966):

$$Q = \frac{2\pi(\text{peak tidal energy stored})}{(\text{energy lost per cycle})}. \quad (1.5)$$

For Earth  $Q \approx 10$ . The fluid nature of the outer planets leads to a larger value of  $Q$ . If Io were torn from the surface of Jupiter 4.5  $\times 10^9$  yr ago, its present position allows the calculation of a lower bound on the time average of  $Q \approx 7 \times 10^4$  (Goldreich & Soter 1966; Yoder & Peale 1981). Recent calculations of the Laplacian resonance of Io, Europa, and Ganymede, the observation of anomalous heat output from Io (Matson, Ransford, & Johnson 1980; Sinton 1981), and estimation of the secular acceleration of Io from the 300 yr record of eclipse observations (Lieske 1987) suggest that  $4 \times 10^4 < Q < 5 \times 10^5$  (cf. Greenberg 1987, 1989; Malhotra 1991), although values as small as  $Q \leq 1.4 \times 10^4$  are possible (Tittlemore 1990). Further, the rather small value of tidal  $Q \approx 10^4$  estimated on Uranus (Tittlemore & Wisdom 1989) strengthens the possibility of  $Q$  being closer to the  $10^4$  bound on Jupiter.

For the case of Earth the astronomical estimates can be accounted for by the dissipation of the ocean tide (although there are still unresolved issues; Platzman 1984). No convincing source of tidal dissipation has been identified for Jupiter and the outer planets. It is clear that equilibrium tide calculations cannot produce the desired values; for example, Goldreich & Soter (1966) estimated the  $Q$  associated with dissipation of the equilibrium tide by eddy viscosity distributed over the top  $10^3$  km of the planet and arrived at  $Q \approx 10^{13}$ . Calculations of the tidal excitation of Jupiter under the assumption of a neutral interior produced a flux  $\approx 10^{11}$  W of gravity wave energy propagating away from the planet, implying  $Q \approx 10^9$  (Houben 1978; Houben & Gierasch 1977). Values closer to the observed are achieved by considering the dissipation of the body tide at the solid core of the planets giving  $Q \approx 10^6$ – $10^7$  (Dermott 1979). Presently the only known mechanism capable of producing tidal dissipation in Jupiter which is consistent with the observed heat output of Io is dissipation of the tidal fields by hysteresis in the tidally induced oscillations of helium raindrops in the planet's interior (Stevenson 1983).

We find that relaxing the assumption of neutrality of the interior allows values of tidal dissipation consistent with evolutionary theory, and in addition the tidal dissipation can reach  $10^{16}$  W resulting in adequate dissipation in Jupiter to account for the volcanism of Io.

In II we have presented the tidal equations for a non-hydrostatic ideal gas atmosphere. In § 2 we extend classical tidal theory to planetary interiors taking into account the effects of sphericity and self-gravity. By ignoring the nonradial component of the rotation vector in the coriolis force (the traditional approximation; Eckart 1960) we arrive at a separable set of equations. We argue that the traditional approximations will be accurate because the dynamic development of tidal disturbances occurs at the outer 10% of the radius of the planet. The meridional structure satisfies the Laplace tidal equation which has been solved in IL.

In § 3 we describe the thermodynamic structure of Jupiter. For simplicity we assume a planetary interior which satisfies a polytropic constitutive relation with index 1. Following Cowling (1941) we allow the existence of static stability in the interior by assuming adiabatic compressibilities  $\Gamma_1 > 2$ . The polytropic interior is matched to an ideal gas atmosphere with the observed temperature above the visible clouds.

In § 4 we present the WKB theory of the vertical structure equation. We delineate the regions for which inertial, gravity, and acoustic oscillations are possible. In § 5 we treat the case of

a planet with a neutral interior. We discuss the various atmospheric boundary conditions and show that the tidal response is small. In § 6 we perform calculations with a stable interior and calculate the corresponding tidal dissipation factor  $Q$ .

## 2. THE EQUATIONS OF SMALL ADIABATIC MOTIONS OF A PLANET

The planet will be modelled as an inviscid adiabatic fluid rotating with constant angular velocity  $\omega$ . We will derive the equations of motion that govern the small adiabatic oscillations about a motionless and spherically symmetric mean state in a frame of reference rotating with the planet. The motion is assumed to be caused by the gravitational tidal potential of a satellite revolving around the planet. Let  $w$ ,  $v$ , and  $u$  denote the radial ( $r$ ), zonal ( $\phi$ ), and meridional ( $\theta$ , the colatitude) component of velocity in spherical coordinates. Let the subscript "o" refer to an equilibrium value of any quantity, and let a symbol without a subscript represent the perturbed part of that quantity.

The equation of continuity, linearized about a motionless and spherically symmetric basic state in hydrostatic balance, is

$$\frac{\partial \rho}{\partial t} + w \frac{d\rho_o}{dr} + \rho_o \chi = 0, \quad (2.1)$$

where  $\rho$  is the density, and  $\chi$  the divergence:

$$\chi = \frac{1}{r^2} \frac{\partial(r^2 w)}{\partial r} + \frac{1}{r \sin \theta} \frac{\partial v}{\partial \phi} + \frac{1}{r \sin \theta} \frac{\partial(u \sin \theta)}{\partial \theta}. \quad (2.2)$$

The linearized thermodynamic equation for adiabatic motion about the hydrostatic mean state is

$$\frac{\partial p}{\partial t} = c^2 \frac{\partial \rho}{\partial t} - \rho_o \frac{c^2}{g_o} N^2 w, \quad (2.3)$$

where  $p$  is the pressure,  $g_o$  the acceleration of gravity due to the mean distribution of mass, and  $c$  the speed of sound:

$$c^2 = \Gamma_1 \frac{p_o}{\rho_o}. \quad (2.4)$$

The Brunt-Väisälä frequency,  $N$ , is given by

$$N^2 = -g_o \left( \frac{d \ln \rho_o}{dr} + \frac{g_o}{c^2} \right). \quad (2.5)$$

The compressibility at constant entropy,  $\Gamma_1 = (d \ln p / d \ln \rho)_s$ , reduces, for an ideal gas, to  $\gamma$ , the ratio of specific heat at constant pressure to that at constant volume. In the interior of the planet and in stellar interiors  $\Gamma_1$  is a variable quantity (Chandrasekhar 1955). However, its variation is relatively small, and we assume  $\Gamma_1$  to be constant in the interior of the planet. Also, note that thermally driven turbulent eddy exchanges have been ignored in equation (2.3).

Combining equations (2.1) and (2.3) we obtain

$$\frac{\partial p}{\partial t} = \rho_o (g_o w - c^2 \chi). \quad (2.6)$$

The gravitational potential consists of an equilibrium part,  $\Phi_o$ , and a perturbed part,  $\Phi$ . They satisfy, separately, the Poisson equations

$$\nabla^2 \Phi_o = 4\pi G \rho_o, \quad \nabla^2 \Phi = 4\pi G \rho, \quad (2.7)$$

with  $G$  the universal constant of gravitation.

We ignore the effect of perturbation density on the gravitational potential. This approximation, due to Cowling (1941), is accurate for motions of higher order meridional and azimuthal structure for which the gravitational potential due to the perturbation density at one part of the fluid cancels that from other parts (Unno et al. 1979). Cowling (1941) provided some justification for ignoring  $\Phi$ , even when the motion is of low meridional and azimuthal order. With the Cowling approximation, the perturbation potential,  $\Phi$ , is externally determined and equal to the tidal potential,  $\Omega_r$ , which is related to its surface value,  $\Omega$ , by

$$\Omega_r = \Omega(\theta) \frac{r^2}{a^2} e^{i\sigma t + is\phi}, \quad (2.8)$$

in which  $\sigma$  is the frequency of the gravitational forcing, and,  $s$ , the zonal wavenumber. The gravitational forcing of Jupiter by Io is primarily semidiurnal with  $s = 2$ . For the values of the frequency and the tidal potential at the surface of the planet refer to IL.

The inviscid momentum equations, neglecting the nonradial component of the rotation vector in the coriolis force (the traditional approximation, Eckart 1960), become

$$\frac{\partial u}{\partial t} - 2\omega \cos \theta v = -\frac{1}{r} \frac{\partial P}{\partial \theta}, \quad (2.9)$$

$$\frac{\partial v}{\partial t} + 2\omega \cos \theta u = -\frac{1}{r \sin \theta} \frac{\partial P}{\partial \phi}, \quad (2.10)$$

$$\rho_o \frac{\partial w}{\partial t} = -\frac{\partial p}{\partial r} - \rho_o \frac{\partial \Omega_r}{\partial r} - g_o \rho, \quad (2.11)$$

in which  $P = p/\rho_o + \Omega_r$  is the reduced pressure. The traditional approximation is accurate for large-scale motions in stable thin spherical shells (Phillips 1966). The traditional approximation could be extended deeper into the planet. Validity of the extension of the approximation into the interior is suggested by the fact that the tidal motions are confined in large measure to the outer layers of the planet. The above approximations, the traditional, the Cowling, and the inviscid, result in major simplification. The equations become separable under these approximations which affords easy and familiar interpretation similar to that in the classical theory of tides (Chapman & Lindzen 1970). The major point of departure from the classical theory is retention of the nonhydrostatic terms in the radial momentum equation (2.11) which become important in the planetary interior when the Brunt-Väisälä frequency is small.

Assume that the tidal response has reached a periodic state under the forcing of the revolving satellite. The dependence of the perturbed quantities on time and azimuthal angle will be the same as that of the forcing which has the form  $e^{i\sigma t + is\phi}$ . We will continue to denote the perturbed quantities with the same symbol as previously, it being understood that the quantities refer to the  $(\sigma, s)$  mode.

Eliminating the horizontal velocities and substituting into the divergence,  $\chi$ , we obtain

$$\chi = \frac{1}{r^2} \frac{\partial(r^2 w)}{\partial r} + \frac{i\sigma}{4\omega^2 r^2} F[P], \quad (2.12)$$

where  $F$  is the Laplace tidal operator, which determines the meridional structure of the tidal fields and which depends only on  $f = \sigma/2\omega$ . For the gravitational forcing of Jupiter by Io this

quantity is  $f = 0.766$  (see IL). Expanding the various fields in terms of Hough functions,  $\Theta_n(\theta)$ , we obtain, that is, for the tidal potential:

$$\Omega_r = \frac{r^2}{a^2} \sum_1^\infty \Omega_n \Theta_n(\theta) e^{i\sigma t + is\phi}. \quad (2.13)$$

The divergence equation (2.12) becomes

$$\chi_n = \frac{1}{r^2} \frac{\partial(r^2 w_n)}{\partial r} - \frac{i\sigma}{g_s h_n} \frac{a^2}{r^2} P_n, \quad (2.14)$$

where the subscript,  $n$ , denotes the order of the Hough mode,  $g_s$ , the gravitational acceleration at the surface of the planet, and  $h_n$  the equivalent depth of the Hough mode. The values of the equivalent depths for Jupiter due to the tidal forcing of Io are derived in IL.

Eliminating the density from equations (2.11) and (2.3) we obtain

$$\xi_n = \frac{(dP_n/dr) - (N^2/g_o)P_n + (N^2/g_o)\Omega_n(r^2/a^2)}{\sigma^2 - N^2}, \quad (2.15)$$

where the radial displacement,  $\xi_n = w_n/i\sigma$ . Eliminating the divergence,  $\chi_n$ , from equations (2.6) and (2.14) gives

$$\frac{1}{r^2} \frac{d(r^2 \xi_n)}{dr} + \left( \frac{1}{c^2} - \frac{1}{g_s h_n} \frac{a^2}{r^2} \right) P_n - \frac{g_o}{c^2} \xi_n = \frac{\Omega_n}{c^2} \frac{r^2}{a^2}. \quad (2.16)$$

We transform equations (2.15) and (2.16) into canonical form by defining

$$\tilde{\xi}_n \equiv r^2 \xi_n \exp\left(-\int_0^r \frac{g_o}{c^2} dr\right), \quad \tilde{p}_n = \frac{P_n}{\rho_o} \exp\left(-\int_0^r \frac{N^2}{g_o} dr\right). \quad (2.17)$$

In terms of the new variables equations (2.15) and (2.16) become

$$\frac{d\tilde{\xi}_n}{dr} = h(r) \frac{r^2}{c^2} \left( \frac{c^2}{g_s h_n} \frac{a^2}{r^2} - 1 \right) \tilde{p}_n + \frac{r^2 \Omega_n}{g_s h_n} \exp\left(-\int_0^r \frac{g_o}{c^2} dr\right), \quad (2.18)$$

$$\frac{d\tilde{p}_n}{dr} = \frac{1}{h(r)r^2} (\sigma^2 - N^2) \tilde{\xi}_n - \frac{2r}{a^2} \Omega_n \exp\left(-\int_0^r \frac{N^2}{g_o} dr\right), \quad (2.19)$$

where

$$h(r) = \exp\left[\int_0^r \left( \frac{N^2}{g_o} - \frac{g_o}{c^2} \right) dr\right]. \quad (2.20)$$

### 3. THE THERMODYNAMIC BASIS STATE OF JUPITER

The planet is taken to be a mixture of hydrogen and helium with a constant abundance of 90%  $H_2$  by mass. The planet's thermodynamic state is taken to be different in the interior of the planet than in the atmospheric envelope (see Fig. 1). The atmosphere is assumed an ideal gas with  $\gamma = 1.4$ . We assume that the gas in the interior of the planet obeys the polytropic constitutive relation

$$p_o = K \rho_o^n, \quad (3.1)$$

with  $K$  a constant to be determined by the mass of the planet,  $M$ , and the requirement that the density vanish at the planet's

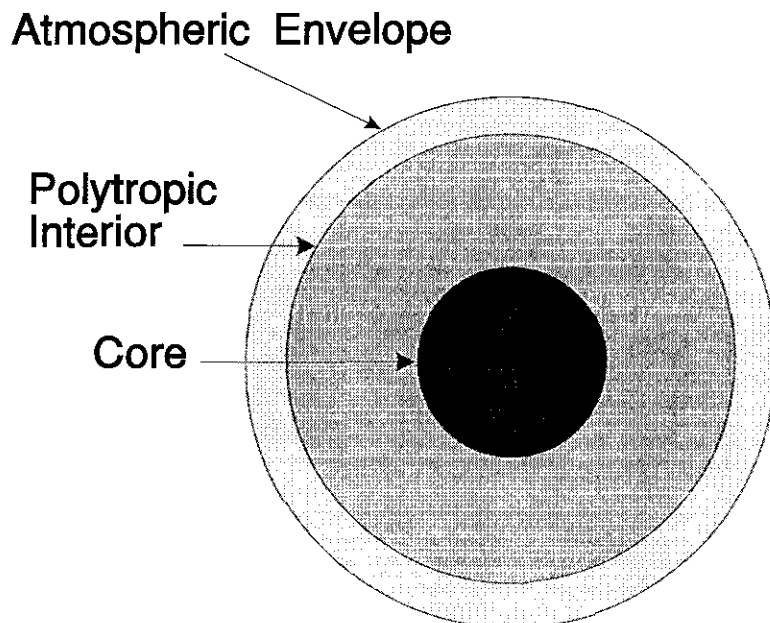


FIG. 1.—Schematic of the different regions of the planet. In the atmospheric envelope we assume the ideal gas law. The polytropic interior obeys  $p_o = K\rho_o^2$ . From the cloud level to the center of the planet there are approximately 18 scale heights. The atmospheric envelope under the visible clouds is 4–10 scale heights deep.

surface ( $r = a$ ) through the solution of

$$\frac{d}{dr} \left( r^2 \rho_o^{n-2} \frac{d\rho_o}{dr} \right) = - \frac{4\pi G}{nK} r^2 \rho_o, \quad (3.2)$$

the Lane-Emden equation (Chandrasekhar 1955).

Early theoretical studies of the interior constitution of the Jovian planets (de Marcus 1958; Öpik 1962) and gravimetric inversions (Hubbard 1974) indicated that the distribution of mass is hydrostatic and to a good approximation consistent with the polytropic constitutive relation with  $n \approx 2$ . On the other hand, work on the high-pressure thermodynamics of hydrogen-helium mixtures (Stevenson 1978; Hubbard & Stevenson 1984) indicated that the adiabatic compressibility parameter  $\Gamma_1$  increases with pressure from the ideal gas value of  $\approx 1.4$  at the atmospheric envelope to  $\approx 3$  for pressures of the order of 1 Mbar, and over a substantial range of pressures is  $\approx 2$ , leading to the conclusion that the polytropic equation of state  $p_o = K\rho_o^2$  is a convenient and an appropriate simplification of the constitutive relation in the interior of the planet. The polytropic relation with  $n = 2$  has the advantage that the distribution of density can be solved in closed form

$$\rho_o(r) = \rho_{oc} \hat{\rho}_o(\eta) = \rho_{oc} \frac{\sin(\pi\eta)}{\pi\eta}, \quad (3.3)$$

where  $\eta = r/a$ ,  $\hat{\rho}_o$  is the normalized density, and the density at the center of the planet is  $\rho_{oc} = \pi M/4a^3$ . The polytropic constant  $K$  is determined to be  $K = 2Ga^2/\pi$ .

The mean density and the mean of pressure are plotted as a function of the radius of the planet in Figures 2 and 3, respectively. The pressure is expressed in terms of the number of scale heights  $x = -\ln(p/p_{\text{cloud}})$ , where  $p_{\text{cloud}}$  is taken to be the pressure at the top of the visible clouds of the planet ( $\approx 300$  mbar). Remarkably, there are only about 18 scale heights from the visible atmospheric envelope to the center of the planet, while there are only four scale heights from  $0.9a$  to the center of the

planet. The tidal response at the atmospheric envelope depends on the number of scale heights spanning the distance between the atmospheric envelope and the levels of excitation primarily concentrated in the interior of the planet (see IL). As a consequence the tidal response will primarily depend on the outermost layers of the planet.

The gravitational acceleration can be derived from the distribution of mass and is given by

$$g_o = -g_s \frac{d\hat{\rho}_o}{d\eta}. \quad (3.4)$$

In Figure 4 we plot the variation of the gravitational acceleration as a function of the radius of the planet.

Although, the interior is taken to obey the polytropic relation with  $n = 2$ , following Cowling (1941) we also allow for  $\Gamma_1 \geq 2$ . When  $\Gamma_1 = 2$  the interior is neutral, that is,  $N = 0$ .

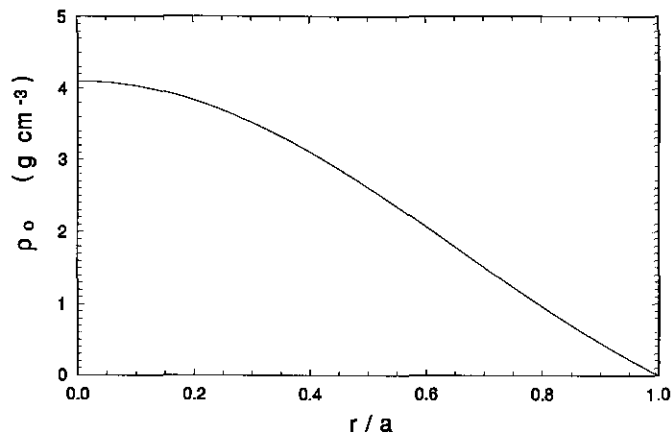


FIG. 2.—Mean density of Jupiter as a function of the fractional radius of the planet. It is calculated for the polytropic interior  $p_o = K\rho_o^2$ .

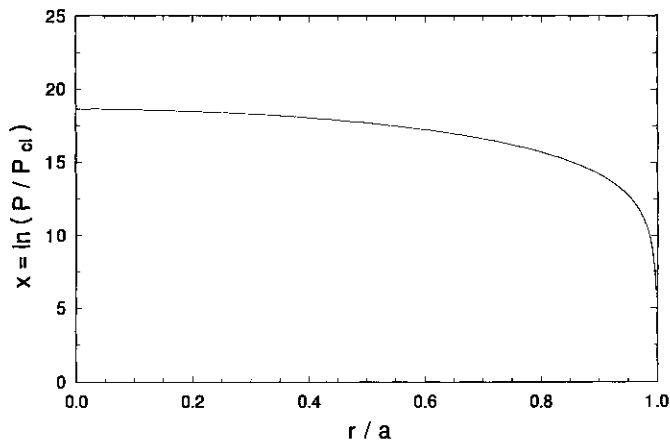


FIG. 3.—Mean pressure of Jupiter as a function of the fractional radius of the planet. It is calculated for the polytropic interior  $p_o = K\rho_o^2$ . The pressure is plotted in terms of the log-pressure coordinate,  $x$ , which indicates the number of scale heights. At the center of the planet the pressure is around 34 Mbar, at the cloud tops is 0.3 bar. Note that there are around 18 scale heights from the visible clouds to the center of the planet, out of which the 15 are between the clouds and 0.9 of the radius of the planet.

When  $\Gamma_1 > 2$  the interior is stably stratified with Brunt-Väisälä frequency given by

$$N^2 = \frac{g_s}{a} \frac{\Gamma_1 - 2}{\Gamma_1} \frac{1}{\hat{\rho}_o} \left( \frac{d\hat{\rho}_o}{d\eta} \right)^2 = \frac{\Gamma_1 - 2}{\Gamma_1} \frac{g_o^2}{\hat{\rho}_o a g_s}, \quad (3.5)$$

and the speed of sound is given by

$$c^2 = \frac{\Gamma_1}{2} g_s a \hat{\rho}_o. \quad (3.6)$$

For Jupiter the distribution of  $N$  in the interior of the planet and in the deep atmosphere is unknown. The existence of an internal heat source leads to the widely accepted view that the interior is in an average state of neutral stability (Hubbard & Smoluchowski 1973; Stevenson & Salpeter 1976). The processes that maintain the mean static stability are complex and poorly understood even for the well-observed terrestrial atmosphere and ocean. In general, it can be argued that if heat from

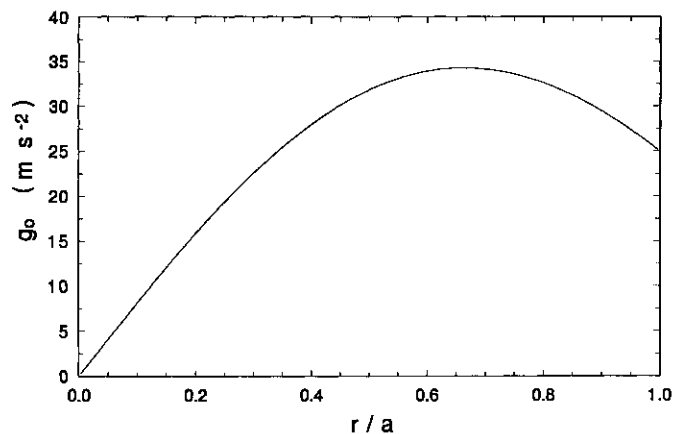


FIG. 4.—Distribution of the gravitational acceleration in Jupiter as a function of the fractional radius of the planet. It is calculated for the polytropic interior  $p_o = K\rho_o^2$ . Note that the maximum acceleration occurs at around 0.7 of the planetary radius.

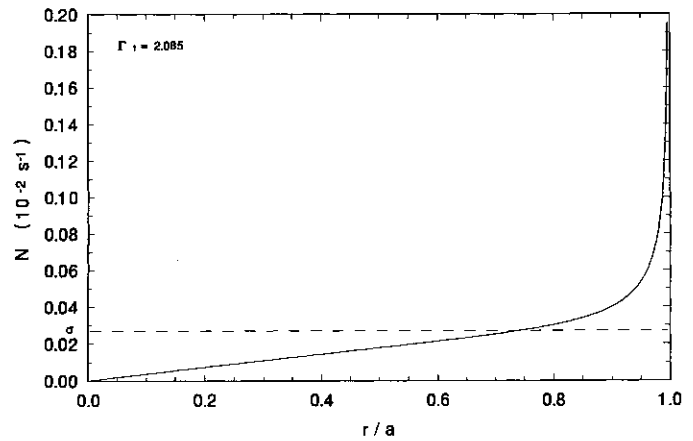


FIG. 5.—Brunt-Väisälä frequency,  $N$ , in the interior of Jupiter, as a function of the fractional radius of the planet. The interior mean state satisfies the polytropic constitutive relation with  $n = 2$  and  $\Gamma_1 = 2.085$ . The dashed line shows the frequency of the external periodic forcing,  $\sigma$ . For comparison, note that at the visible cloud level  $N \approx 65 \sigma$ .

the interior is supplied to the surface by thin convective plumes, the interior must maintain an average positive static stability if the compressional heating in the downwelling regions is to be balanced by loss of heat (Lindzen 1977). We show in the next sections that the inclusion of even small positive static stability in the interior of the planet has a dramatic effect on the tidal response at the atmospheric envelope. In this sense, the study of the tidal response of the planet with a neutrally buoyant mean state is dynamically singular. Note that low levels of static stability, although dynamically significant, may be difficult to detect by direct measurement of  $N$ .

The idealized distribution of  $N$  in the interior of the planet which is given by equation (3.6) is shown in Figure 5 for  $\Gamma_1 = 2.085$ . Note the rapid decrease of  $N$  caused by the rapid increase of density with radius and the eventual vanishing of the gravitation acceleration at the center of the planet; for  $r/a < 0.75$  we find  $N < \sigma$ . At the atmospheric envelope  $N$  is of the order of  $2 \times 10^{-2} \text{ s}^{-1}$  which is  $\approx 65 \sigma$  at the 100 mbar level (see Achterberg & Ingersoll 1990). Note that  $N > \sigma$  is necessary for oscillations to behave as vertically propagating waves (cf. § 4). Note as well that at the outer parts of the planet, below the atmospheric envelope,  $N < 10 \sigma$ , a value of static stability which may be hard to distinguish observationally from neutrality.

To estimate the possible range of values of the compressibility parameter  $\Gamma_1$  let us first assume that the idealized distribution of  $N$ , equation (3.6), is valid up to the visible region of the atmospheric envelope of Jupiter. In this case, the  $\Gamma_1$  that matches the observed lapse rate of about  $2 \text{ K km}^{-1}$  at the atmosphere is 2.56. We will instead assume an atmospheric thermal state, adapted from Achterberg & Ingersoll (1990), which places the transition from the ideal gas atmosphere to the polytropic interior at 4–10 scale heights below the visible clouds (details of this construction are presented in Appendix A). Generally we assume that the static stability rapidly decreases in the deep atmosphere of the planet above the polytropic interior, but we consider the possibility of the existence of local regions of higher stability (i.e., due to compositional differentiation or disequilibrium of the parastates and orthostates of molecular hydrogen) as suggested by the arguments of Conrath & Gierasch (1984) and Gierasch & Conrath (1987).

Under these conditions a large range of values of  $\Gamma_1$ , that is,  $2.01 < \Gamma_1 < 2.15$ , is consistent with continuous transition from the atmosphere to the polytropic interior.

#### 4. QUALITATIVE DESCRIPTION OF TIDAL MOTION

Assume slow variation of the coefficients of the radial structure equations (2.18)–(2.19) so that we can perform a WKB analysis. Under this assumption, we obtain the local dispersion relation

$$\kappa_R^2 = \left( \frac{c^2}{g_s h_n} \frac{a^2}{r^2} - 1 \right) \frac{(N^2 - \sigma^2)}{c^2}. \quad (4.1)$$

with  $\kappa_R$  the radial wavenumber.

The equivalent depth,  $h_n$ , can be used to obtain an estimate of the horizontal wavenumber. Consider a rotating planar channel at colatitude  $\theta$  with local coriolis parameter  $f_o = 2\omega \cos \theta$  (Lindzen 1990). The Laplace tidal equation for this planar channel gives

$$g_s h_n = \frac{\sigma^2 - f_o^2}{\kappa_{H,s}^2}, \quad (4.2)$$

with  $\kappa_{H,s}$  the total horizontal wavenumber (in units of inverse length) at the surface of the planet. Note that smaller equivalent heights correspond to higher horizontal wavenumbers. The horizontal wavenumber at the surface is related to the horizontal wavenumber at any radius  $r$ ,  $\kappa_H$ , by

$$\kappa_{H,s} = \kappa_H \frac{r}{a}. \quad (4.3)$$

The geometrical constraint requires for a given horizontal wavenumber at the surface of the planet,  $\kappa_{H,s}$ , that  $\lim_{r \rightarrow 0} \kappa_H = \infty$ . With equation (4.3) the dispersion relation takes the form

$$\kappa_R^2 = \left( \frac{c^2 \kappa_H^2}{\sigma^2 - f_o^2} - 1 \right) \frac{(N^2 - \sigma^2)}{c^2}. \quad (4.4)$$

describing all the possible mixed internal gravity, inertial, and acoustic oscillations. Consider  $c \rightarrow \infty$  to reduce equation (4.4) to the familiar dispersion relation for inertia-gravity oscillations:

$$\frac{\kappa_H^2}{\kappa_R^2} = \frac{\sigma^2 - f_o^2}{N^2 - \sigma^2}. \quad (4.5)$$

To have propagation it is necessary to have either  $N \geq \sigma \geq f_o$  or  $N \leq \sigma \leq f_o$ . The former condition is expected to be satisfied in the atmospheric envelope of the planet for some waves of positive equivalent depth (recall from equation [4.2] that  $h_n > 0$  is associated with  $\sigma > f_o$ ). In the interior of the planet and for modes of positive equivalent depth we expect trapping unless the stratification is sufficiently strong, which happens only at the outer layers of the planet. A plot of  $\kappa_R^2 a^2$  (nondimensionalized by the radius of the planet  $a$ ) is shown in Figure 6 for Jupiter for various equivalent heights for a neutral interior ( $\Gamma_1 = 2.00$ ) and an interior with some stability ( $\Gamma_1 = 2.01$ ). Note that the modes of positive equivalent depth, which can amplify at the atmospheric envelope, will be strongly trapped in the deep interior of the planet regardless of the value of  $\Gamma_1$ . At the outer parts of the planet, where the stratification is significant, only the higher order Hough modes can propagate in accord with the discussion in IL.

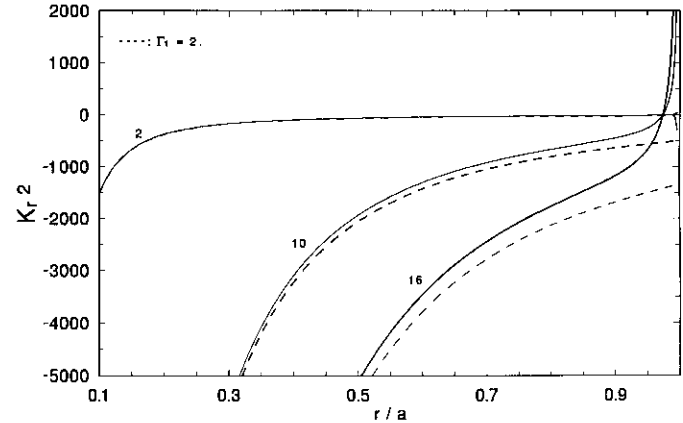


FIG. 6.—Square of radial wavenumber (made nondimensional by multiplying with the radius of the planet,  $a$ , as a function of the fractional radius of the planet Jupiter). The solid curves show the wavenumber for a planet with  $\Gamma_1 = 2.01$  in the interior for the second Hough mode (marked with a 2), the tenth Hough mode (marked with a 10), and the sixteenth Hough mode (marked with a 16). The dashed curves show the corresponding values for a neutral interior ( $\Gamma = 2.0$ ). Propagation is possible when the square of the wavenumber is positive. The presence of stability allows the higher positive equivalent depth modes to propagate. This occurs at the outer layers of the planet. The tenth Hough mode has equivalent depth of approximately 949 km, the tenth Hough mode 29 km, the sixteenth 11 km.

In the interior and for  $N \leq \sigma \leq f_o$ , only the Hough modes with negative equivalent depth can propagate. These modes, confined to the poles of the planet, will be trapped in the stable atmospheric envelope but in the interior will be propagating inertial waves. The wavelength of these inertial oscillations decreases toward the center of the planet. It can be shown that neglect of the nonradial component of planetary vorticity is inappropriate near the center of the planet. To avoid this singularity at the center of the planet, we appeal to the probable existence of a core at  $r_{\text{core}} \approx 0.13a$  (Stevenson 1978; Hubbard & Stevenson 1984) and limit the integration of the equations to  $r > r_{\text{core}}$ .

To delineate the acoustic branch consider equation (4.4) with  $N^2 = 0$

$$\kappa_R^2 = \left( 1 - \frac{c^2 \kappa_H^2}{\sigma^2 - f_o^2} \right) \frac{\sigma^2}{c^2}. \quad (4.6)$$

Propagation of acoustic waves is prohibited in the deep interior by the large value of the speed of sound and of the horizontal wavenumber,  $\kappa_H$  (see eq. [4.3]). A typical distribution of the sound speed in relation to the angular velocity as a function of Jupiter's radius is shown in Figure 7; for comparison the phase speeds of the corresponding equivalent gravity waves are tabulated in Table 1. Note that the speed of sound in the interior exceeds the phase speed of the equivalent gravity waves. Consequently, for frequencies characteristic of tidal forcing, the acoustic branch does not modify the propagation characteristics already derived from the dispersion relation of the inertia-gravity waves given by equation (4.5). Exceptionally, in the outer layers of the plane (i.e.,  $r > 0.96a$ ) acoustic propagation is possible by the lowest order Hough modes. For example, for a neutral planet,  $\Gamma_1 = 2.00$ , the gravest Hough mode can acoustically propagate at the outermost edges of the planet, while the tenth and the sixteenth mode are everywhere trapped in the interior of the planet (see Fig. 6). Note that for

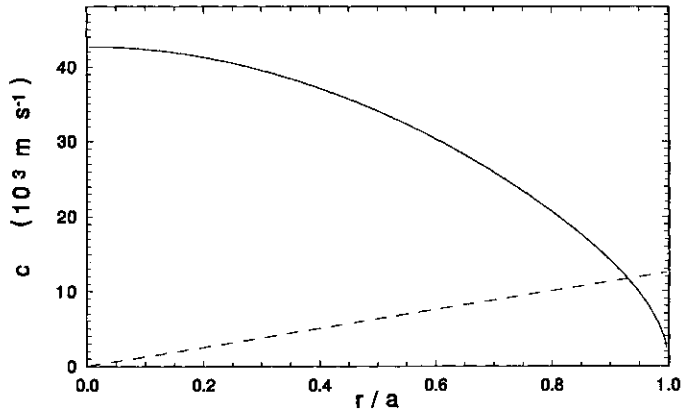


FIG. 7.—Speed of sound  $c$  for a polytrope of index 2. The dashed curve is the linear speed due to the rotation of the planet as a function of the planetary radius.

$\Gamma_1 = 2.01$  the gravest Hough mode develops an acoustic duct at the outer edges of the planet.

5. TIDAL OSCILLATIONS IN A PLANET WITH A NEUTRAL INTERIOR

The radial structure equation, expressed in terms of reduced pressure, becomes for a planet with a neutral interior ( $\Gamma_1 = 2$ )

$$\frac{d^2 P_n}{d\eta^2} + \left( \frac{2}{\eta} + \frac{1}{\hat{\rho}_o} \frac{d\hat{\rho}_o}{d\eta} \right) \frac{dP_n}{d\eta} + \frac{\sigma^2 a}{g_s} \left( \frac{1}{\hat{\rho}_o} - \frac{a}{h_n \eta^2} \right) P_n = \frac{\sigma^2 a \eta^2}{g_s \hat{\rho}_o} \Omega_n, \tag{5.1}$$

with  $\eta = r/a$ , the relative distance, and  $\hat{\rho}_o$ , the normalized mean density. The radial displacement is given by  $\xi_n = 1/\sigma^2 dP_n/dr$ .

To specify the boundary condition at the surface of the planet ( $\eta = 1$ ) let us assume that equation (5.1) is valid everywhere in the planet, that is, the stability is neutral even at the shallow atmospheric envelope. The outer boundary condition is then constant pressure at the outer material surface. This condition, linearized about  $\eta = 1$ , is

$$P_n - \xi_n g_o \rho_o = 0, \tag{5.2}$$

TABLE 1  
JUPITER  
 $f = 0.766, s = 2$

Hough Mode	$h_n$ (km)	$c_g [(g_s h_n)^{1/2}]$ (m s <sup>-1</sup> )
2.....	948.9	4870.8
4.....	204.5	2261
6.....	85	1457.4
8.....	46.1	1073.25
10.....	28.8	848.9
12.....	19.7	701.9
14.....	14.3	598.3
16.....	10.9	521.3
18.....	8.5	461.8
20.....	6.87	414

NOTES.—The equivalent heights,  $h_n$ , and the equivalent gravity wave speed,  $c_g$ , for the first 10 symmetric Hough modes of Jupiter, corresponding to the tidal forcing of the planet by Io.

which in terms of reduced pressure takes the form

$$-\frac{dP_n}{d\eta} \Big|_{\eta=1} + \frac{\sigma^2 a}{g_s} P_n \Big|_{\eta=1} = \frac{\sigma^2 a}{g_s} \Omega_n. \tag{5.3}$$

Note that as  $\eta \rightarrow 1$ ,  $\hat{\rho}_o \approx 1 - \eta$  and  $d\hat{\rho}_o/d\eta \rightarrow -1$  (for the outer planets  $\sigma^2 a/g_s \approx 0.1$ ). Equation (5.1) has a regular singular point at  $\eta = 1$ . However, because the singular terms are identical to the pressure boundary condition (5.3), the interior solution of equation (5.1) develops no boundary layer at the surface to satisfy the outer boundary condition.

To determine the outer boundary condition in the presence of a stable atmosphere, consider the radial structure equation for the shallow and isothermal atmospheric envelope with  $N > \sigma$ :

$$\frac{d^2 P_n}{dx^2} - \frac{dP_n}{dx} + \kappa \frac{H}{h_n} P_n = 0, \tag{5.4}$$

where  $x = r/H$ , and  $H$ , the scale height, is given by  $H = RT/g_s$ , with  $R$ , the gas constant per unit mass,  $T$  the skin temperature of the atmospheric envelope, and  $\kappa = \gamma - 1/\gamma$ . The atmospheric outer boundary condition (see IL) leads to the solution of equation (5.4),  $P_n = C e^{\lambda x + x^2/2}$ , with

$$\lambda = \begin{cases} i(\kappa H/h_n - 1/4)^{1/2} & \text{if } \kappa H/h_n - 1/4 > 0 \\ -(1/4 - \kappa H/h_n)^{1/2} & \text{if } \kappa H/h_n - 1/4 < 0 \end{cases} \tag{5.5}$$

in which  $C$  is a constant to be determined by the continuity of pressure and displacement at the interface separating the neutral interior satisfying equation (5.1) from the stable atmospheric envelope. Denote the interior variables by “ $i$ ” and the corresponding atmospheric variables by “ $a$ .” The conditions at the interface are

$$P_n^i = P_n^a, \quad -\frac{dP_n^i}{d\eta} + \frac{\sigma^2 a}{g_s} P_n^i - \frac{\sigma^2 a}{g_s} \Omega_n = \frac{\sigma^2 a}{g_s \kappa} \frac{dP_n^a}{dx}. \tag{5.6}$$

The outer boundary condition is given either by equation (5.3) or (5.6). The lower boundary condition is zero displacement at the inner core.

To investigate the effect of these boundary conditions on the solutions we integrate equation (5.1) for various outer boundary conditions and with the inner core located at different radii. The resulting radial distribution of pressure, radial velocity, and zonal velocity are shown respectively in Figures 8, 9, and 10. The results are not sensitive to either boundary condition. It has been shown in § 4 that all Hough modes with positive equivalent depth are strongly trapped in the interior of the planet (see Fig. 6). This results is the observed insensitivity to the lower boundary condition. Note that modes with negative equivalent depth propagate in the interior, but are trapped in the atmosphere.

It is informative to define the equilibrium radial displacement of a material surface under the influence of the external tidal potential,  $\Omega_e$ :  $\xi_{\text{equilib}} = -\Omega_e/g_o$ . The radial displacement and the equilibrium displacement are shown in Figure 11 as a function of the radius of the planet. The effectiveness of the forcing in exciting tides in the planetary atmosphere is proportional to the difference between the two displacements, because the tidal fields are forced by this geopotential disequilibrium. For example, if the inner planet were separated by a solid interface from the atmosphere, atmospheric tides would result from the response to the forcing of 13 m geopotential disequilibrium at the ground (for Earth the corresponding

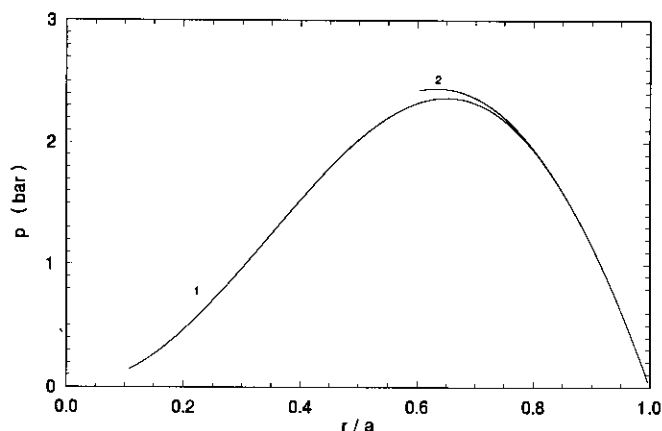


FIG. 8.—Magnitude of perturbation pressure at the equator as a function of the radius due to the tidal excitation of planet Jupiter by its satellite Io. The interior is exactly neutral. The phase is almost 0 and is in phase with the displacement of the equilibrium tide. The pressure is measured in bar (1 bar =  $10^5$  Pa), and the radius as a fraction of the planetary radius  $a$ . Curve 1 shows the response when a solid boundary (i.e., a core) has been placed at  $0.1a$  and the atmospheric envelope is an isothermal atmosphere of temperature 160 K. The three indistinguishable curves identified as “2” correspond to the integration with a solid boundary at  $0.6a$  and (1) an isothermal atmospheric envelope at 160 K, (2) an isothermal atmospheric envelope at 220 K, and (3) no atmosphere. This calculation, as well as all the others to follow, was performed with the first 14 symmetric Hough modes of positive equivalent depth, and the first 10 symmetric Hough modes of negative equivalent depth.

value is 20 cm which corresponds to a hydrostatic tidal pressure fluctuation of  $20 \mu\text{bar}$ ; the observed gravitational tidal pressure fluctuation is approximately  $60 \mu\text{bar}$ ). Instead the neutral interior reduces the geopotential forcing to 30–100 cm. This is to be expected because, with the absence of gravitational restoring force, the weak compressional and inertial restoring forces cannot oppose the imposed geopotential deformation. Remarkably, a planet with neutral interior has tiny tidal response, while introduction of small stability in the interior leads to greatly enhanced dynamic displacements:  $\xi - \xi_{\text{equilib}} \approx 20$  m. Previous calculations (Houben 1978; Houben & Gierasch 1977) treated a neutral interior and consequently produced small tidal forcing in the atmosphere and a resulting tidal dissipation factor  $Q \approx 10^9$ , which is four to five orders of magnitudes larger from the values required for

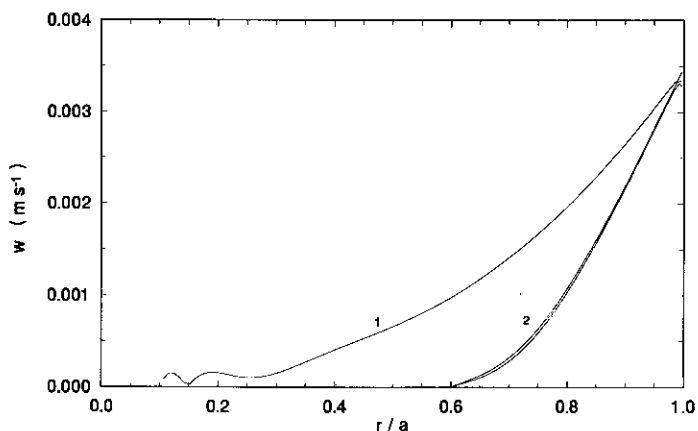


FIG. 9.—Magnitude of the radial velocity at the equator of Jupiter as a function of the fractional radius of the planet. The interior is exactly neutral. The curves correspond to the same cases as in Fig. 8.

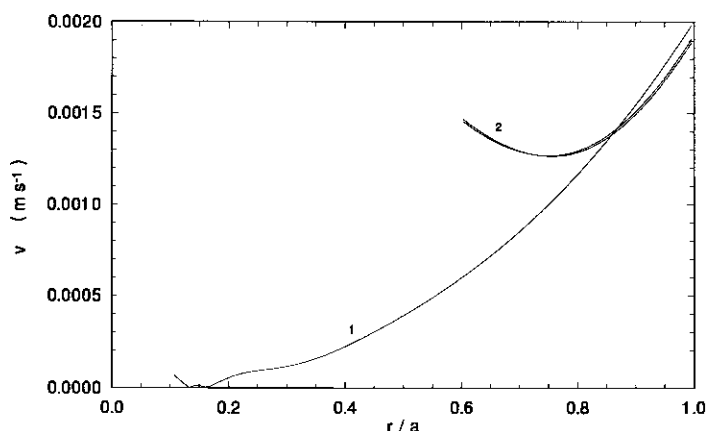


FIG. 10.—Magnitude of the zonal (westerly) velocity as a function of fractional radius for various boundary conditions of Fig. 8. The interior has been assumed neutral.

orbital evolution. We can, however, produce a tidal  $Q$  consistent with the constraints set by orbital evolution theory by assuming that the planetary interior has nonzero stability.

#### 6. ESTIMATION OF TIDAL EXCITATION AND DISSIPATION IN A PLANET WITH A STABLE INTERIOR

Consider a planet with some stability in the interior. The solution in the planetary interior is matched to the atmospheric solution which obeys (see IL)

$$\frac{d^2 y_n}{dx^2} + \left[ \frac{N^2 H^2}{g_s h_n} + \frac{\sigma^2 H}{\gamma g_s} \left( 1 - \frac{\gamma H}{h_n} \right) - \frac{1}{4} \right] y_n = 0, \quad (6.1)$$

where  $y_n = \chi_n e^{-x/2}$ , and  $x \equiv \int_0^z dz/H$ .

We assume the observed temperature structure above the visible clouds (refer to Appendix A). In this region only Hough modes of order  $n > 12$  can propagate. Below the clouds the static stability is assumed to decrease exponentially at such a rate that all the Hough modes are trapped. Transition to the polytropic interior takes place at about nine scale heights below the visible clouds, and in the interior the static stability

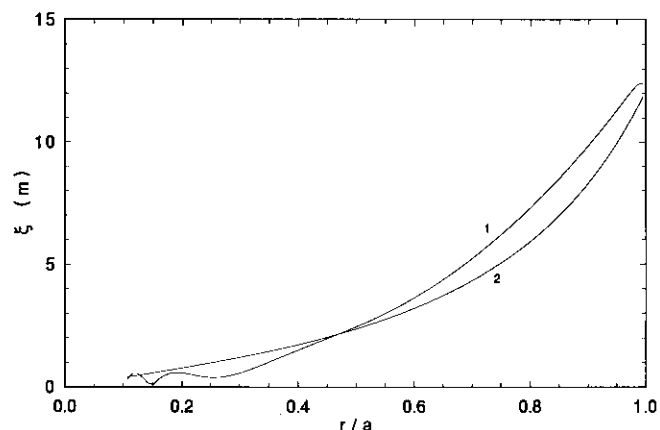


FIG. 11.—Magnitude of the radial displacement as a function of the fractional radius. Curve 1 is the radial displacement calculated from the dynamic response in Jupiter, the interior is exactly neutral, and the core has been placed at 0.1 of the planetary radius. Curve 2 is the radial displacement of the equilibrium tide.

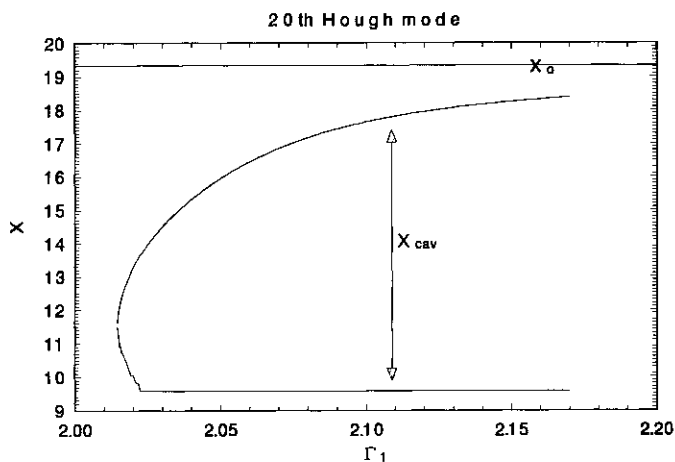


FIG. 12.—Location of the waveguide in the planetary interior for the twentieth Hough mode ( $h_{20} = 6.87$  km) as a function of  $\Gamma_1$ . The location,  $X$ , is specified by the number of scale heights below the visible clouds.  $X_o$  corresponds to the center of the planet. The polytropic planetary interior starts at  $X \approx 9$ .

is given by equation (3.6) with  $\Gamma_1 > 2$ . Propagation of the higher Hough modes is possible in the outer parts of the planetary interior. Deeper into the planet all the modes with positive equivalent depth are trapped, and only those with negative equivalent depth can propagate. To clarify the influence of the static stability in the planetary interior we allow a discontinuity at the interface separating the polytrope from the ideal gas atmosphere. Note that introduction of some stability in the interior leads to formation of the waveguide, in accordance with the discussion in § 4. The structure of the assumed static stability is not crucial for the creation of this duct. Note that formation of a waveguide, for a given Hough mode, requires values of  $N$  in inverse proportion to the local scale height.

We first present the radial structure of a single Hough mode as a function of  $\Gamma_1$ , choosing for definiteness the twentieth mode. The location, marked by the number of scale heights below the visible clouds, of the resulting waveguide in the planetary interior as function of  $\Gamma_1$  is shown in Figure 12. As  $\Gamma_1$  varies, the waveguide becomes resonant with the driving potential. To test the numerical solutions, and the accuracy of the WKB approximations of § 4, we calculate the resonant  $\Gamma_1$  from the WKB quantization condition:

$$\int_{r_1}^{r_2} \kappa_R dr = (n + \frac{1}{2})\pi, \quad (6.2)$$

where  $\kappa_R$  is the radial wavenumber, given by equation (4.1), and  $r_1$  and  $r_2$  the limits of the waveguide. The response of the atmospheric envelope as a function of  $\Gamma_1$  is shown in Figure 13. The WKB analysis is accurate even for the first resonant mode.

The strength of the tidal fields in the atmosphere is estimated by the resulting radiation energy flux,  $\overline{pw}$ . This energy flux represents the power radiated away from the planet and can provide an estimate for the associated tidal dissipation factor  $Q$  through use of equation (1.5). The peak energy of the tidal fields is calculated as the maximum potential energy of the tide in the planetary interior (Houben & Gierasch 1977; Houben 1978). Note that the resulting magnitude of  $Q$ , although indicative, is certainly an overestimate because neither the dissipation of the trapped modes nor other forms of dissipation have been taken into account. The dependence of the energy flux and the associated  $Q$  are plotted in Figure 14 as a function of  $\Gamma_1$  for the twentieth Hough mode. If we disregard the resonant peaks, we note that the amplitude of the tidal fields for  $\Gamma_1 > 2.02$  asymptotes to a value which is two to three orders (recalling that the flux is a quadratic quantity) of magnitude larger than the resulting fields with a neutral interior. This asymptotic behavior is caused by the slow increase of the number of scale heights as the waveguide extends deeper than  $\approx 0.9a$  of the planet. Also note that as the stability in the interior increases from neutrality the atmospheric response will reach a minimum before approaching its asymptotic value.

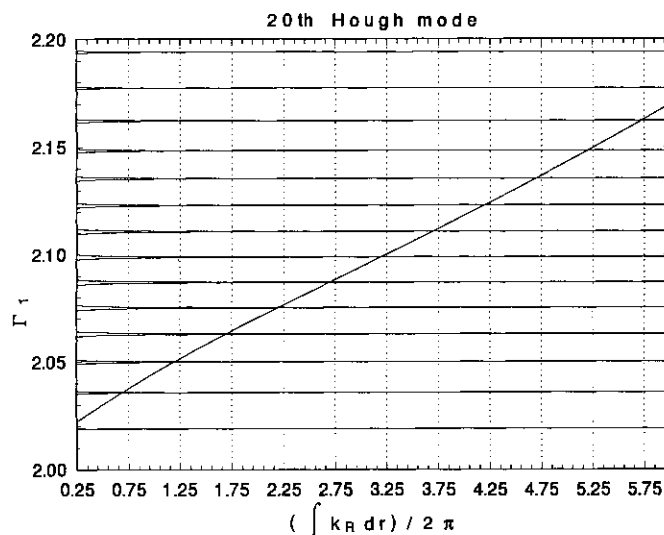


FIG. 13.—Resonant  $\Gamma_1$  according to WKB theory and the numerical calculation for the twentieth Hough mode. The dotted lines correspond to  $(n + 1/2)/2$ ,  $n = 1, 2, \dots$ ; the slanted continuous line is  $\int \kappa_R dr / 2\pi$  as a function of  $\Gamma_1$ . The points of intersection between these two lines specify the resonant  $\Gamma_1$  according to WKB theory. The horizontal spikes show the radial velocity in  $\text{m s}^{-1}$  at 10 scale heights above the visible clouds as a function of  $\Gamma_1$ ; the values are the result of numerical integration. Note the accuracy of the WKB theory.

ation of the trapped modes nor other forms of dissipation have been taken into account. The dependence of the energy flux and the associated  $Q$  are plotted in Figure 14 as a function of  $\Gamma_1$  for the twentieth Hough mode. If we disregard the resonant peaks, we note that the amplitude of the tidal fields for  $\Gamma_1 > 2.02$  asymptotes to a value which is two to three orders (recalling that the flux is a quadratic quantity) of magnitude larger than the resulting fields with a neutral interior. This asymptotic behavior is caused by the slow increase of the number of scale heights as the waveguide extends deeper than  $\approx 0.9a$  of the planet. Also note that as the stability in the interior increases from neutrality the atmospheric response will reach a minimum before approaching its asymptotic value.

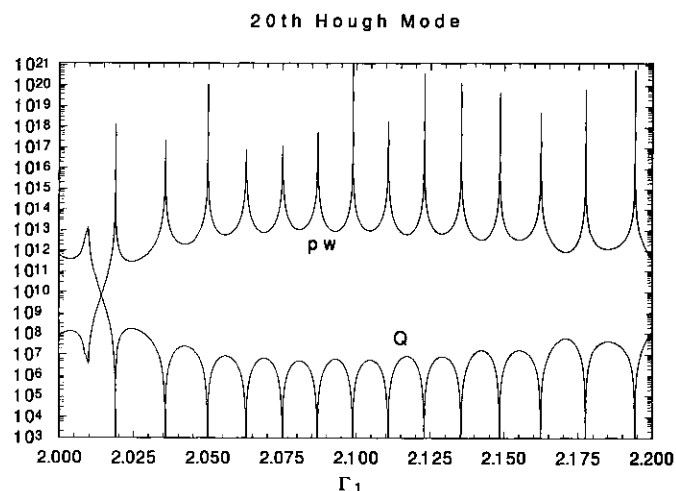


FIG. 14.—Energy flux  $\overline{pw}$  in watts, integrated over the surface of the planet at the visible atmosphere for the twentieth Hough mode, as a function of  $\Gamma_1$ . The lower curve shows the corresponding  $Q$ .

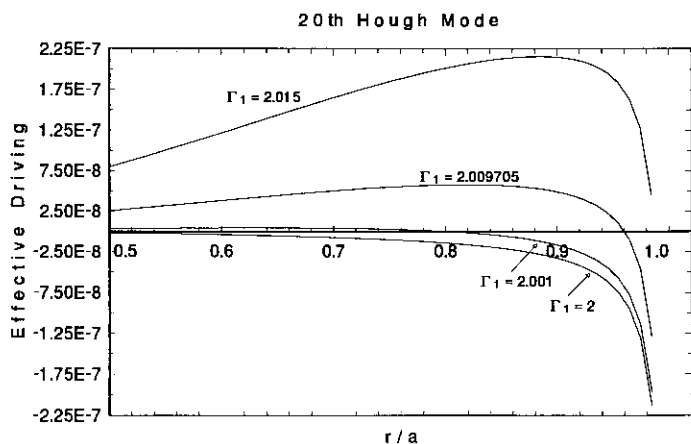


FIG. 15.—Effective forcing as a function of the radius of the planet for various  $\Gamma_1$ . The values are made nondimensional by  $g_s a$ .

This is due to the effect of the structure of the distributed tidal forcing in the interior. The effective forcing in the interior, derived by combining equations (2.18) and (2.19) into a single equation for the radial displacement, will depend on the thermodynamic structure of the planetary interior as discussed in § 5. The structure of the effective forcing as a function of the radius of the planet is shown in Figure 15 for various  $\Gamma_1$ . We notice that for a neutral interior the effective forcing is in phase with the driving tidal potential. For very small static stability the driving is out of phase with the effective forcing in the deep interior and in phase at the outer parts of the planet, leading to a reduced response. For  $\Gamma_1 > 2.015$  the effective forcing is everywhere out of phase with the driving, indicating that the frequency of the tidal driving is less than the neutral period of the restoring force of the medium.

Consider the response of the interior when the total tidal driving is taken into account. The resulting magnitude of the dynamic displacement  $\xi - \xi_{\text{equilib}}$  at the equator of the planet is shown in Figure 16. Note the substantial departure from equilibrium displacement indicating an energetic response of the atmosphere. The resulting energy flux and the associated  $Q$

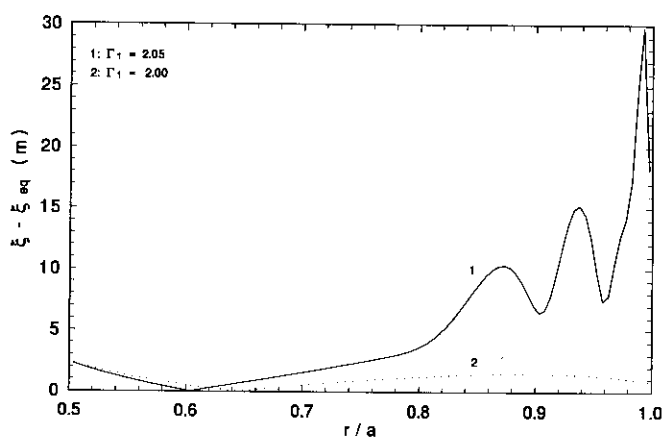


FIG. 16.—Magnitude of the difference between the dynamic radial displacement and the equilibrium radial displacement at the equator as a function of the fractional radius of the planet Jupiter. The tidal response of the atmospheric envelope is proportional to the disequilibrium of the dynamic response. Curve 1 represents the response of an interior with some stability ( $\Gamma_1 = 2.05$ ); curve 2 represents the case of an exactly neutral interior.

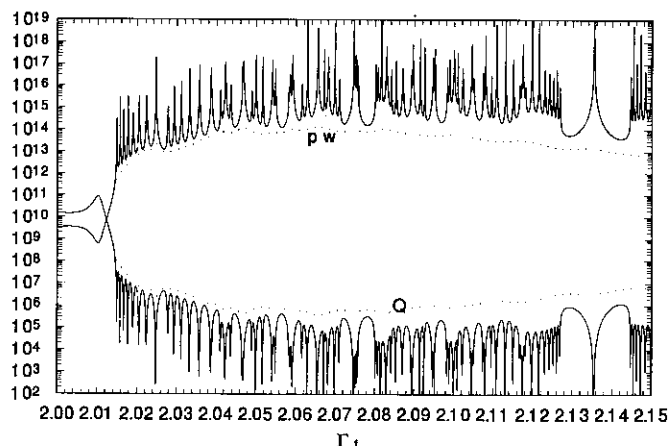


FIG. 17.—Total energy flux  $\overline{pw}$  in watts, integrated over the surface of the planet at the visible atmosphere, as a function of  $\Gamma_1$ . Only the Hough modes ( $n \geq 12$ ) which propagate in the upper atmosphere contribute to the energy flux. The lower curve shows the corresponding  $Q$ . The dotted curves show the corresponding results with an effective dissipation in the planetary interior of 60 hr.

as a function of  $\Gamma_1$  are shown in Figure 17. The resonant peaks indicate the selective resonance of different Hough modes. As we remarked in IL, the tidal driving, which is proportional to the second spherical harmonic, projects on many Hough modes, each of which can separately resonate. The resonant peaks can be suppressed by introduction of adequate dissipation in the interior. Dissipation can be simulated by allowing the forcing frequency  $\sigma$  to assume complex values. For large interior dissipation the resonances are diffuse. Such a case with an interior dissipation time scale of 60 hr is shown in Figure 17.

Disregarding the resonant peaks, the tidal response asymptotes to an energy flux level of  $\approx 3 \times 10^{14}$  W over the whole surface of Jupiter which corresponds to  $\approx 0.005$  W m $^{-2}$ . The associated  $Q$  asymptotes to  $\approx 10^5$  in accord with the value expected from astronomical arguments. Note that if the dissipation in the interior is small, so that the resonances are sharp, the energy flux can reach the order of  $10^{17}$ – $10^{18}$  W. These large energy fluxes result in values of  $Q$  of the order of  $10^3$ . That such a situation is plausible is indicated by the anomalous heat output of Io (Yoder & Peale 1981). In the case of reduced interior dissipation the tidal fields in the atmosphere may show a discernible episodic signature caused by the time variations of the interior stability. It is then plausible that tidally forced wave fields reach an energy comparable to the thermal emission of Jupiter ( $14$  W m $^2$  which is  $\approx 10^{17}$  W).

## 7. CONCLUSIONS

We have extended the classical theory of tides, reviewed in IL, to study the tidal response of a deep fluid planetary body. We have retained the separation of the meridional and vertical structure equations by neglecting the horizontal components of the rotation vector in the calculation of the coriolis acceleration. We expect this approximation to give accurate results and even prove useful in determining the free modes of a rapidly rotating planet.

The tidal response is found to crucially depend on the distribution of static stability in the interior. The presence of convection in the planetary interior has often been assumed to

lead to a state of neutral stability. While absolute neutrality in the interior is a good first approximation to determine the mean thermodynamic state, small departures from neutrality have important implications for the tidal response. The tidal response of the atmospheric envelope is proportional to the departure of the tidal fields from their equilibrium value. In the absence of any stability in the interior a neutrally buoyant material surface deforms and becomes nearly an equilibrium equipotential surface leading to small tidal excitation.

We have shown that the presence of some small static stability at the outer parts of the planet leads to dramatic enhancement of tidal response in the atmosphere. The tidal fields are then capable of radiating enough energy away from the planet to result in a tidal dissipation factor  $Q$  consistent with the bounds set by astronomical considerations. The presence of static stability in the planetary interior creates ducts in which the various Hough modes can resonate. If the viscous dissipation is not very large in the planetary interior, we expect this resonant behavior to result in episodically very large tidal activity as the interior stability is modulated by convection. If we disregard the resonant peaks, the tidal activity quickly asymptotes to a value which is independent of the amount of stability and is consistent with the tidal dissipation required by the astronomical arguments.

We have utilized a very simple model for the static stability in which the most stable layers are concentrated in the outer parts of the planet, but are separated by a nine scale height deep neutrally buoyant region below the clouds. We expect our conclusions to apply also to more structured models of interior static stability, as long as the static stability is not concentrated too deep in the interior. Remarkably, the assumption of a rigorously neutral interior is dynamically singular, and,

encouraged by agreement with astronomically determined tidal dissipation, we are led to the hypothesis that the interior of the planet should possess some static stability. Verification of the hypothesis must await sufficiently accurate observations of the tidal response of Jupiter.

If a forthcoming paper we will present the detailed structure of the tidal response in the visible atmosphere as a function of the static stability of the planetary interior. We have already found that the tidally forced wave fields may produce an energy flux comparable to the thermal emission of Jupiter ( $\approx 10^{17}$  W). This energy flux may be associated with a source of momentum that can maintain the puzzling observed cloud level mean zonal circulation of the planet. Using the Eliassen-Palm theorem (Lindzen 1990) we can estimate the expected latitudinally averaged acceleration of the mean flow to be  $\approx 10^{-2} \text{ m s}^{-1} \text{ day}^{-1}$  assuming that the momentum of the waves is deposited in a layer of one scale height in depth (25 km). However, the interaction of vertically propagating and vertically trapped modes can lead to a latitudinal redistribution of zonal angular momentum on the scale of the dominant vertically propagating Hough mode (Fels & Lindzen 1974). These alternating local accelerations will be concentrated in restricted latitude bands suggestively resembling the visible banding of the planet. Detailed calculation of the implied mean zonal accelerations will be presented in a forthcoming paper.

This work was supported by NASA NAGW-525 and by NSF ATM 91-4441. We thank Peter Gierasch for informing us of the thesis by Houben. The authors thank Brian Farrell for valued assistance.

## APPENDIX

### THE CONSTRUCTION OF THE MEAN STATE

The temperature of the visible part of the atmosphere is taken to simulate observations on Jupiter (Lindal et al. 1981). Following Lindzen (1970) it is expressed as

$$T(x) = T_0 + c_1 \frac{x}{2} + \sum_{i=1}^{i=2} \delta_i \frac{c_{i+1} - c_i}{2} \ln \left[ \frac{\cosh(x - x_i/\delta_i)}{\cosh(x_i/\delta_i)} \right], \quad (\text{A1})$$

with  $T_0 = 110$  K the minimum temperature above the clouds which is taken to occur at a pressure  $p_0 = 145$  mbar. The vertical distribution is expressed as a function of

$$x = -\ln \frac{p}{p_0} = \int_0^z \frac{dz}{H(z)}, \quad (\text{A2})$$

where  $x$  is the log-pressure coordinate, and  $H$  the local scale height as a function of distance from the altitude where the minimum temperature occurs which is designated the  $z = 0$  level. The cloud tops are one-to-two scale heights below the minimum of the temperature. Temperature distribution (A1) holds for  $x \geq 0$  and agrees with the observed distribution when we take  $c_1 = 0$ ,  $c_2 = 18.011$ ,  $c_3 = 0$ ,  $x_1 = 0$ ,  $x_2 = 2.63$ ,  $\delta_1 = 4$ , and  $\delta_2 = 4$  (see Fig. 18).

For the region  $x \geq 0$  the Brunt-Väisälä frequency  $N^2$  is calculated from distribution (A1) and

$$N^2 = \frac{g_s}{H} \left( \kappa + \frac{1}{H} \frac{dH}{dx} \right), \quad (\text{A3})$$

$$\kappa = \frac{\gamma - 1}{\gamma}. \quad (\text{A4})$$

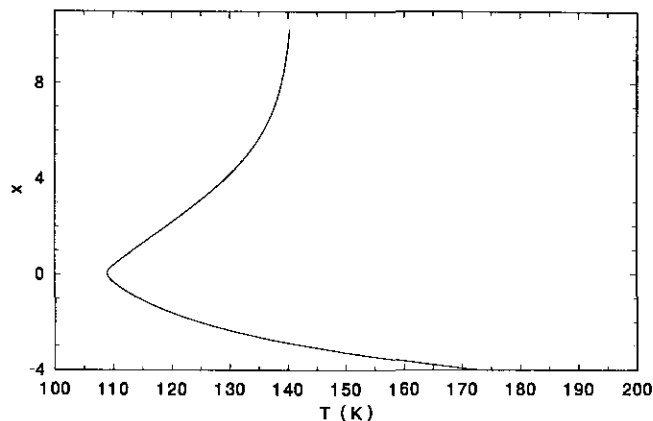


FIG. 18

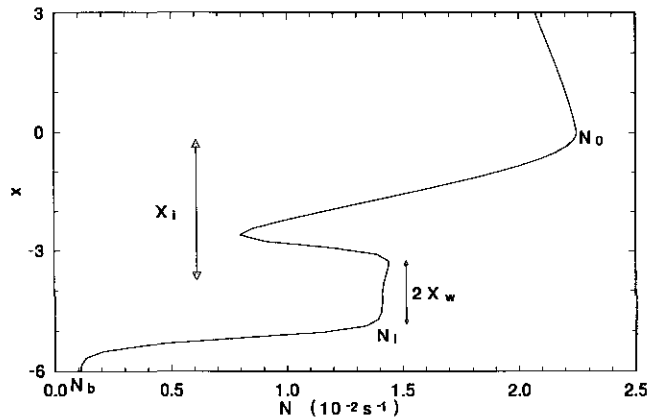


FIG. 19

FIG. 18.—Temperature distribution as a function of the log-pressure coordinate  $x$ . The cloud tops correspond to around  $x = -1$ . The temperature profile for  $x > 0$  is taken from observations (Lindal et al. 1981). Under the cloud tops we have assumed that the static stability decreases toward neutrality.

FIG. 19.—Static stability in the atmospheric envelope as a function of the log-pressure coordinate,  $x$ . The temperature minimum is taken as the reference level where  $x = 0$ . The maximum in the static stability,  $N_p$ , under the cloud tops is located at  $X_i$  and has a width of  $2X_w$ .  $N_0$  refers to the static stability at the reference level, while  $N_b$  is the static stability at the base of the atmospheric envelope, just above the transition to the interior polytrope. For the calculations presented in this paper we have taken  $N_i = 0$ .

For the region  $0 > x > X_p$ ,  $X_p$  the level of transition of the polytropic interior, we consider the following distribution of Brunt-Väisälä frequency

$$N^2 = (N_0^2 - N_b^2) \exp\left(-\frac{x^2}{\delta_0}\right) + N_b^2 + N_i^2 \left[ \tanh\left(\frac{x - X_i + X_w}{\delta_i}\right) - \tanh\left(\frac{x - X_i - X_w}{\delta_i}\right) \right], \quad (\text{A5})$$

where  $N_0$  is the frequency at level  $x = 0$ ,  $N_i$  the maximum frequency of an interior hump in Brunt-Väisälä frequency of width  $2X_w$  at a level  $X_i$ , and  $N_b$  the Brunt-Väisälä frequency at the base of the atmospheric envelope at the level of transition to the polytropic interior (see Fig. 19).

The temperature distribution in  $x < 0$  is derived by inverting equation (A3) up to  $X_p$ , the level of transition to the polytropic interior. The transition to the polytropic interior is determined as the level where the density and pressure of the mean state are the same as the ideal gas density and pressure  $X_p$  scale heights below the temperature minimum at  $x = 0$ . The pressure and density distribution is determined by integrating equation (A3) and using the hydrostatic relation and the ideal gas law. The transition level  $X_p$  depends on the distribution of the static stability. To allow for greater flexibility we gradually increase the value of  $\gamma$  in this region to 1.6. At the visible atmosphere  $\gamma = 1.4$ .

At the transition level to the polytropic interior we also require  $N_b^2 > N_p^2$ , that is, Brunt-Väisälä frequency just above the transition to the interior is greater than the Brunt-Väisälä frequency in the interior at the point of transition to the atmospheric envelope. Solving equation (3.6) we can thus determine an upper bound for  $\Gamma_1$ .

As we noted, we can easily construct ducts to resonate the various Hough modes. Here we present two examples of a resonant duct in the atmosphere. For a duct that resonates the tenth Hough mode take  $\delta_0 = 0.4$ ,  $\delta_i = 0.2$ ,  $N_b = 5\sigma$ ,  $N_i^2 = 0.5380 N_0^2$ , and  $X_w = 1.1$ . Matching with the interior places the beginning of the polytropic region at  $X_p = 6.29$  under the temperature minimum, and  $X_i = 4.35 - X_p$ . For  $\Gamma_1 = 2.015741$  the static stability is continuous at the interface between the polytropic interior and the ideal gas atmosphere.

For the sixteenth Hough mode the duct is well separated from the cloud layer lying deeper in the interior. The parameters for resonance are as follows:  $\delta_0 = 3$ ,  $\delta_i = 0.2$ ,  $N_b = 5\sigma$ ,  $N_i^2 = 0.069150001 N_0^2$ ,  $X_w = 0.05$ . Matching with the interior sets the beginning of the polytropic region at  $X_p = 10.3$ , and  $X_i = 9.40 - X_p$ . For  $\Gamma_1 = 2.1145$  the static stability is continuous at the interface between the polytropic interior and the ideal gas atmosphere.

## REFERENCES

- Achterberg, R. K., & Ingersoll, A. P. 1990, *J. Atm. Sci.*, 46, 2448  
 Chandrasekhar, S. 1955, *An Introduction to the Study of Stellar Structure* (New York: Dover)  
 Chapman, S., & Lindzen, R. S. 1970, *Atmospheric Tides* (Dordrecht: Reidel)  
 Conrath, B. J., & Gierasch, P. J. 1984, *Icarus*, 57, 184  
 Cowling, G. T. 1941, *MNRAS*, 101, 367  
 Darwin, G. H. 1910, in *Encyclopaedia Britannica*, Vol. 26, Eleventh Edition (New York), 938  
 De Marcus, W. C. 1958, *AJ*, 63, 2  
 Dermott, S. F. 1979, *Icarus*, 37, 310  
 Eckart, C. 1960, *Hydrodynamics of Oceans and Atmospheres* (London: Pergamon)  
 Fels, S., & Lindzen, R. S. 1974, *Geophys. Fluid Dyn.*, 6, 149  
 Gierasch, P. J., & Conrath, B. J. 1987, *J. Geophys. Res.*, 92, 15019  
 Goldreich, P., & Soter, S. 1966, *Icarus*, 5, 375  
 Greenberg, R. 1987, *Icarus*, 70, 334  
 ———. 1989, in *Time Varying Phenomena in the Jovian System*, ed. M. J. S. Belton, R. A. Weston, & J. Rahe (Washington: NASA), 100  
 Houben, H. C. 1978, Ph.D. thesis, Cornell Univ.  
 Houben, H., & Gierasch, P. J. 1977, in *Proc. Symp. on Planetary Atmospheres*, R. Soc. Canada, 79  
 Hubbard, W. B. 1974, *Icarus*, 1, 200  
 Hubbard, W. B., & Smoluchowski, R. 1973, *Space Sci. Rev.*, 14, 599  
 Hubbard, W. B., & Stevenson, D. J. 1984, in *Saturn*, ed. T. Gehrels & M. S. Matthews (Tucson: Univ. Arizona Press), 395  
 Ingersoll, A. P. 1990, *Science*, 248, 308  
 Ioannou, P. J., & Lindzen, R. S. 1993, *ApJ*, 406, 252 (IL)  
 Ledoux, P., & Walraven, T. 1958, in *Handbuch der Physik*, LI (Berlin: Springer), 353  
 Lieske, J. H. 1987, *A&A*, 176, 146

- Lindal, G. F., et al. 1981, *J. Geophys. Res.*, 86, 8721  
Lindzen, R. S. 1970, *Geophys. Fluid Dyn.*, 1, 303  
———. 1977, in *Problems of Stellar Convection* (Berlin: Springer), 128  
———. 1990, *Dynamics in Atmospheric Physics* (Cambridge: Cambridge Univ. Press)  
———. 1991, *Geophys. Astrophys. Fluid Dyn.*, 58, 123  
Malhotra, R. 1991, *Icarus*, 94, 399  
Matson, D. L., Ransford, G. A., & Johnson, T. V. 1980, *J. Geophys. Res.*, 86, 1664  
Öpik, E. J. 1962, *Icarus*, 1, 200  
Phillips, N. A. 1966, *J. Atm. Sci.*, 23, 626  
Platzman, G. W. 1984, *Rev. Geophys. Space Phys.*, 22, 73  
Sinton, W. M. 1981, *J. Geophys. Res.*, 86, 3122  
Stevenson, D. J. 1978, in *The Origin of the Solar System*, ed. S. F. Dermott (Tucson: Univ. Arizona Press), 395  
———. 1983, *J. Geophys. Res.*, 88, 2445  
Stevenson, D. J., & Salpeter, E. E. 1976, in *Jupiter*, ed. N. Gehrels (Tucson: Univ. Arizona Press), 85  
Tittmore, W. C. 1990, *Science*, 250, 263  
Tittmore, W. C., & Wisdom, J. W. 1989, *Icarus*, 78, 63  
Unno, W., Osaki, Y., Ando, H., & Shibahashi, H. 1979, *Nonradial Oscillations of Stars* (Tokyo: Univ. Tokyo Press)  
Yoder, C. F., & Peale, S. J. 1981, *Icarus*, 47, 1